
01 Jan 2023

Antioxidant Theranostic Copolymer-Mediated Reduction In Oxidative Stress Following Traumatic Brain Injury Improves Outcome In A Mouse Model

Aria W. Tarudji

Connor C. Gee

Hunter A. Miller

Rylie Steffen

et. al. For a complete list of authors, see https://scholarsmine.mst.edu/matsci_eng_facwork/3208

Follow this and additional works at: https://scholarsmine.mst.edu/matsci_eng_facwork

 Part of the [Materials Science and Engineering Commons](#)

Recommended Citation

A. W. Tarudji et al., "Antioxidant Theranostic Copolymer-Mediated Reduction In Oxidative Stress Following Traumatic Brain Injury Improves Outcome In A Mouse Model," *Advanced Therapeutics*, Wiley Open Access, Jan 2023.

The definitive version is available at <https://doi.org/10.1002/adtp.202300147>

This Article - Journal is brought to you for free and open access by Scholars' Mine. It has been accepted for inclusion in Materials Science and Engineering Faculty Research & Creative Works by an authorized administrator of Scholars' Mine. This work is protected by U. S. Copyright Law. Unauthorized use including reproduction for redistribution requires the permission of the copyright holder. For more information, please contact scholarsmine@mst.edu.


Antioxidant Theranostic Copolymer-Mediated Reduction in Oxidative Stress Following Traumatic Brain Injury Improves Outcome in a Mouse Model

Aria W. Tarudji, Connor C. Gee, Hunter A. Miller, Rylie Steffen, Evan T. Curtis, Aaron M. Priester, Anthony J. Convertine, and Forrest M. Kievit*

Following a traumatic brain injury (TBI), excess reactive oxygen species (ROS) and lipid peroxidation products (LPOx) are generated and lead to secondary injury beyond the primary insult. A major limitation of current treatments is poor target engagement, which has prevented success in clinical trials. Thus, nanoparticle-based treatments have received recent attention because of their ability to increase accumulation and retention in damaged brain. Theranostic neuroprotective copolymers (NPC3) containing thiol functional groups can neutralize ROS and LPOx. Immediate administration of NPC3 following injury in a controlled cortical impact (CCI) mouse model provides a therapeutic window in reducing ROS levels at 2.08–20.83 mg kg⁻¹ in males and 5.52–27.62 mg kg⁻¹ in females. This NPC3-mediated reduction in oxidative stress improves spatial learning and memory in males, while females show minimal improvement. Notably, NPC3-mediated reduction in oxidative stress prevents the bilateral spread of necrosis in male mice, which is not observed in female mice and likely accounts for the sex-based spatial learning and memory differences. Overall, these findings suggest sex-based differences to oxidative stress scavenger nanoparticle treatments, and a possible upper threshold of antioxidant activity that provides therapeutic benefit in injured brain since female mice benefit from NPC3 treatment to a lesser extent than male mice.

A. W. Tarudji, C. C. Gee, H. A. Miller, R. Steffen, E. T. Curtis, F. M. Kievit
Department of Biological Systems Engineering
University of Nebraska – Lincoln
262 Morrison Center, Lincoln, NE 68583, USA
E-mail: fkievit2@unl.edu

A. M. Priester, A. J. Convertine
Department of Materials Science and Engineering
Missouri University of Science and Technology
223 McNutt Hall, Rolla, MO 65409, USA

 The ORCID identification number(s) for the author(s) of this article can be found under <https://doi.org/10.1002/adtp.202300147>

© 2023 The Authors. Advanced Therapeutics published by Wiley-VCH GmbH. This is an open access article under the terms of the Creative Commons Attribution-NonCommercial-NoDerivs License, which permits use and distribution in any medium, provided the original work is properly cited, the use is non-commercial and no modifications or adaptations are made.

DOI: 10.1002/adtp.202300147

1. Introduction

Traumatic brain injury (TBI) occurs in two separate injury phases. The primary injury is the initial impact from an external mechanical force that causes axonal shearing, cell membrane disruption, and cell death. Following the primary injury, a cascade of biochemical derangements, such as the release of excitatory amino acids, the influx of calcium ions, and oxidative stress cause further cell death and progression of the injury. This secondary injury can last decades post-injury^[1] and spread to the contralateral hemisphere.^[2]

Under physiological conditions, reactive oxygen species (ROS) are produced in cellular respiration and are balanced by endogenous antioxidant enzymes.^[3] However, following TBI, ROS production is elevated and induces damage to DNA, proteins, and lipids that manifest through DNA oxidation and lipid peroxidation products (LPOx) resulting in neuroinflammation and neurodegeneration.^[4] Thus, ROS and LPOx have become major therapeutic targets in hopes of improving outcomes

following TBI. Several antioxidant and LPOx inhibitor treatments, including polyethylene glycol (PEG)-conjugated superoxide dismutase, PEG-conjugated catalase, tirilazad, and their combinations, have shown promising results in reducing secondary injury in preclinical studies and Phase I and II trials.^[5] Despite the success in preclinical studies and over 30 clinical trials, no TBI drug treatment has received FDA approval for reducing the secondary spread of injury.^[4b,6] The lack of success of TBI clinical trials is multifold, including patient variability and biomarker selection, but treatment timing and poor target engagement of therapeutic agents due to low accumulation and retention in the brain is a major shortcoming that we aim to address.

Nanoparticles (NPs) have emerged as a promising approach for TBI treatment, especially as the blood-brain barrier (BBB) is disrupted following TBI.^[7] The size of NPs is ideal for accumulating in brain injury; NPs are small enough that they can pass through a disrupted BBB similarly to small molecule drugs, but are large enough to be retained in the injury lesion, unlike small molecule drugs.^[7a,8] We recently reported on the

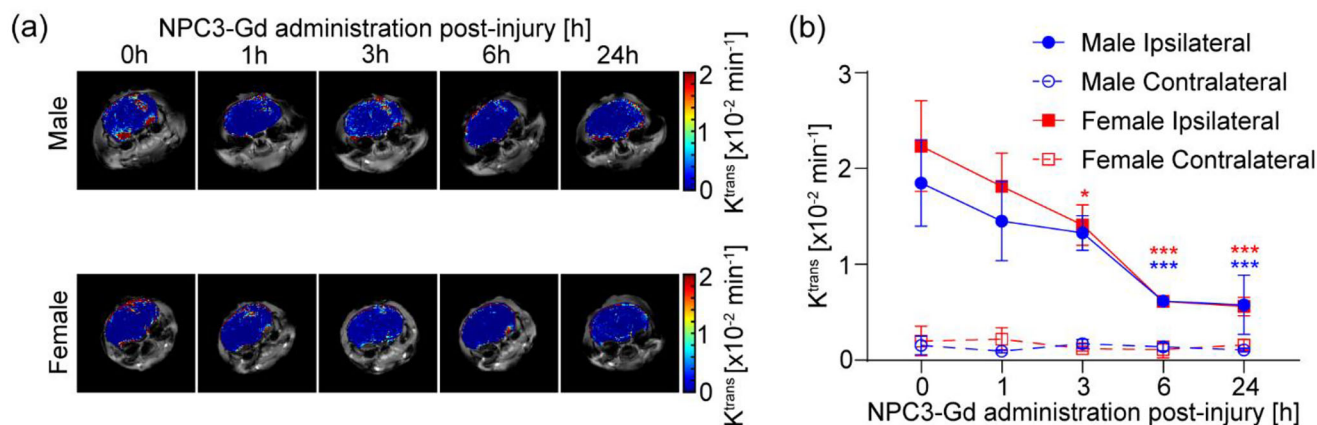


Figure 1. Identifying the treatment window of NPC3. K^{trans} of NPC3-Gd in male and female CCI mouse models of TBI in the lesion and contralateral hemisphere when administered at 0, 1, 3, 6, and 24 h post-injury. a) Representative K^{trans} maps overlaid on structural images of NPC3-Gd administered at 0, 1, 3, 6, and 24 h time points following CCI in male and female mice. b) Quantification of K^{trans} mapping in the lesion. NPC3-Gd accumulated in the lesion the most when administered immediately following the injury (0 h post-injury). Data are shown as mean \pm SD with $n = 3$ for each treatment group, except $n = 5$ for female mice with 0- and 1-h post-injury groups. * indicates a statistical difference compared to 0 h post-injury group, with one and three symbols indicating $p < 0.05$ and $p < 0.001$, respectively, as determined by one-way ANOVA and Dunnett's post hoc test.

development of theranostic neuroprotective copolymers (NPC3) containing functional thiol groups that can bind and inactivate both ROS and LPOx.^[9] NPC3 was developed through reversible addition–fragmentation chain-transfer (RAFT) polymerization and was equipped with PEG to reduce immune recognition and increase blood half-life circulation. Another part of the monomer was functionalized with reduced lipoic acid for the self-assembling of the NPs, as well as the thiol functional group that scavenges ROS and LPOx. With a size of 9 nm, the size of NPC3 is ideal for the accumulation and retention of NPs in TBI. Due to the similar size with macromolecules and NPs, NPC3 is expected to accumulate in the brain injury when administered at 3 d post-injury, and is expected to have a retention half-life in the brain injury for 14 h compared to the retention half-life of small molecule of 4 h.^[8a,8c,8k,9] However, the effect of NPC3 on outcomes is still unknown. Furthermore, our recent results with antioxidant enzyme loaded nanoparticles suggest there are important sex-based differences in the therapeutic efficacy of antioxidant treatments.^[10] Indeed, female humans and rodents are more likely to have a better outcome following severe TBI.^[11] Sexual dimorphism in TBI has been attributed to progesterone, but progesterone treatment did not show significant improvement in TBI patients.^[12] Furthermore, female mice show a higher accumulation of macromolecules and NPs when administered 24 h following TBI.^[8k] Thus, a better understanding of sex-based differences following antioxidant NP treatment will help in the design of next-generation therapeutics to improve outcomes following TBI.

2. Results

2.1. Identifying the Treatment Window of NPC3

To evaluate the accumulation and treatment window of NPC3 in the lesion, we injected CCI mice with Gd-labeled NPC3 NPs (NPC3-Gd) at 0, 1, 3, 6, and 24 h post-injury (Figure 1). Since NPC3 and NPC3-Gd have very similar physical properties (Table 1), we assume the same treatment window profile between oxidative stress scavenger NPC3 and MR contrast agent NPC3-Gd without oxidative stress capacity. We then took a series of T1 images before and up to 45 min post-NPC3-Gd injection with MRI to measure K^{trans} , a permeability coefficient that describes the kinetics of the NPs entering the brain from circulation.^[8b] This provides an advantage over measuring the peak concentration in the brain since the time to reach peak concentration in the brain may change based on time after injury. Thus, the K^{trans} parameter indicates the permeability of the BBB to NPC3 where a higher K^{trans} would indicate an eventual higher maximum brain concentration of NPC3 regardless of when that maximum brain concentration was reached post-injection. We observed the highest accumulation of NPC3-Gd in the lesion when injected immediately following the injury in both male (mean \pm SD = $18.35 \pm 4.5 \times 10^{-3} \text{ min}^{-1}$) and female ($22.20 \pm 4.74 \times 10^{-3} \text{ min}^{-1}$) mice, followed by 1 and 3 h post-injury (male: $14.75 \pm 4.51 \times 10^{-3} \text{ min}^{-1}$ and $13.13 \pm 1.05 \times 10^{-3} \text{ min}^{-1}$; female: $17.98 \pm 3.49 \times 10^{-3} \text{ min}^{-1}$ and $13.95 \pm 2.12 \times 10^{-3} \text{ min}^{-1}$). However, there was a significant reduction in the accumulation of NPC3-Gd in the lesion at 6 and

Table 1. Properties of NPC3 and NPC3-Gd used for K^{trans} imaging and antioxidant therapy (parts of the data were taken from ref^[9]).

Particle	Size [nm]	PDI	Zeta potential [mV]	H ₂ O ₂ scavenging capacity [μmol]	LPOx scavenging capacity [μmol]	Gd concentration [mmol mg ⁻¹ NPC3]
NPC3-Gd	8	0.21	-12.11	~	~	26.73×10^{-6}
NPC3	9	0.16	-10.34	0.25	0.07	~

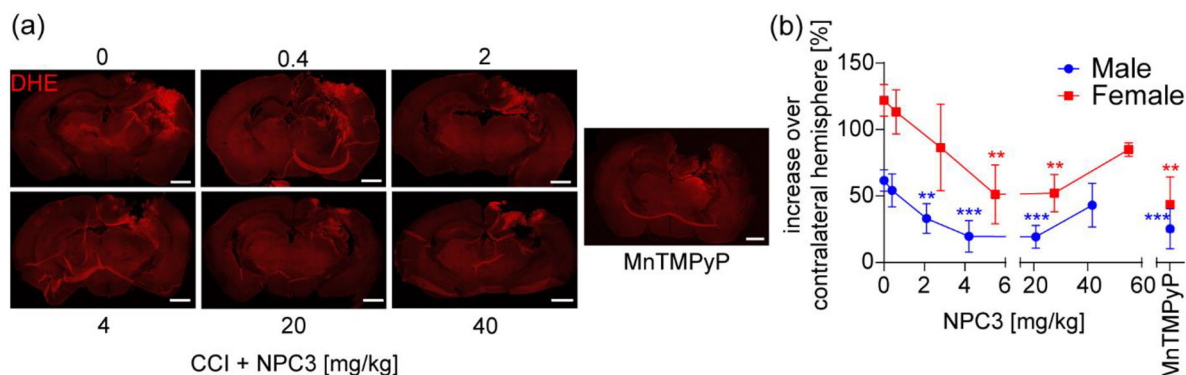


Figure 2. Comparison of the therapeutic window of NPC3 between male and female CCI mice. In vivo DHE staining of the brains at 4 h post-injury was utilized to measure the ROS level in the acute phase of injury. a) Representative confocal microscopy images from various doses of NPC3 and MnTMPyP following CCI. Scale bar is 1 mm. b) Quantification of DHE fluorescence mean intensity in the lesion normalized to the contralateral hemisphere. Data are shown as mean \pm SD with $n = 3$ for female mice treatment groups, and $n = 5$ for male mice treatment groups. * indicates a statistical difference compared to the 0 mg kg^{-1} NPC3 group, with two and three symbols indicating $p < 0.01$ and $p < 0.001$, respectively, as determined by one-way ANOVA and Dunnett's post hoc test.

24 h post-injury (male: $6.01 \pm 0.33 \times 10^{-3} \text{ min}^{-1}$ and $5.62 \pm 1.78 \times 10^{-3} \text{ min}^{-1}$; female: $5.99 \pm 0.33 \times 10^{-3} \text{ min}^{-1}$ and $5.46 \pm 0.55 \times 10^{-3} \text{ min}^{-1}$), compared to the immediate administration of NPC3-Gd. At 24 h post-injury, we still observed a significantly higher accumulation of NPC3-Gd in the lesion compared to the contralateral hemisphere in female mice (3.77 fold higher, $p = 0.0032$), as well as a trending higher in male mice (6.23 fold higher, $p = 0.057$), as determined by student t-test. Based on the arterial input function, the blood elimination half-life of NPC3-Gd was 25.8 min in males and 17.7 min in females (Figure S1, Supporting Information).

2.2. Identifying the Therapeutic Window of NPC3

Finding the highest accumulation of NPC3 in the lesion when injected immediately following the injury (0 h time point), we evaluated the treatment window of NPC3 in scavenging ROS when administered at this time point. We utilized in vivo dihydroethidium (DHE) staining to measure ROS level in the lesion and determine ROS reduction following NPC3 treatment. We injected a series of NPC3 concentrations (100 μL of 0–10 mg mL^{-1} NPC3 in PBS) through tail vein for both male and female mice, which translated to 0, 0.4, 2.1, 4.2, 20.8, and 41.7 mg kg^{-1} in male mice with an average weight of 24 g and 0, 0.6, 2.8, 5.5, 27.6, and 55.2 mg kg^{-1} in female mice with an average weight of 18.1 g. We measured the DHE fluorescence mean intensity using confocal microscopy in the lesion and normalized it to the DHE fluorescence mean intensity in the contralateral hemisphere (Figure 2). Although this method is semi-quantitative, it provides a strong indication of the therapeutic window of NPC3. We observed the highest increase in DHE mean intensity in the untreated CCI mice (0 mg kg^{-1} NPC3) in both male (mean \pm SD = $61.7 \pm 7.96\%$ increase) and female ($121.9 \pm 11.93\%$ increase) mice. DHE mean intensity was significantly reduced with 2.1, 4.2, and 20.8 mg kg^{-1} NPC3 in male mice (46.44%, 68.02%, and 68.64% decrease, respectively), and 5.5 and 27.6 mg kg^{-1} NPC3 in female mice (58.04% and 57.19% decrease, respectively) compared to the 0 mg kg^{-1} NPC3 group. We observed no sig-

nificant reduction in the DHE mean intensity at 41.7 mg kg^{-1} NPC3 in males (30.11% decrease, $p = 0.1027$) and 55.2 mg kg^{-1} NPC3 in females (30.39% decrease, $p = 0.1374$) compared to the 0 mg kg^{-1} NPC3 group. The negative return in the ROS scavenging at 41.7 and 55.2 mg kg^{-1} NPC3 might be caused by the cytotoxicity of NPC3,^[9] in which NPC3 concentrations of greater than 1 mg mL^{-1} were found to reduce cell viability on SH-SY5Y neuron cells. However, our previous studies with nanoparticles similar to NPC3 did not show an adverse effect on body weight and motor function in mice.^[2b,13] Thus, we did not expect any adverse effect of NPC3 in vivo, especially when administered at $\approx 10 \text{ mg kg}^{-1}$ NPC3 (maximum concentration in the blood of $\approx 0.08 \text{ mg mL}^{-1}$ following i.v. injection). From the in vivo DHE assay, we found a wide treatment window of NPC3 of 2.1–20.8 mg kg^{-1} in male mice and 5.5–27.6 mg kg^{-1} in female mice. Another possible reason for the bell-shaped response curve might be due to the physiological role of oxidative stress, in which suboptimal dosing of antioxidants would give a suboptimal reduction in oxidative stress or even exacerbate the injury progression.^[10,14]

Since the therapeutic windows of males and females were studied separately (Figure 2B), small differences in dose between sexes should not act as a confounding variable in this study. Thus, 8.3 mg kg^{-1} NPC3 was chosen for male mice, and 11 mg kg^{-1} NPC3 was chosen for female mice, as the middle point for measuring the reduction of LPOx and SBDPs with NPC3 treatment, as well as the spatial learning and memory in Barnes maze trials. We found that manganese(III) tetrakis(1-methyl-4-pyridyl)porphyrin (MnTMPyP), a small molecule ROS scavenger positive control, has similar efficiency in reducing ROS to the NPC3 when injected immediately following the injury in male and female mice (59% and 64% decrease, respectively).

2.3. Barnes Maze in Male and Female Mice Following TBI

Following our finding of the treatment and therapeutic windows for NPC3 in male and female mice, we next tested the ability of NPC3 dosed within these windows ($\approx 10 \text{ mg kg}^{-1}$ through the tail

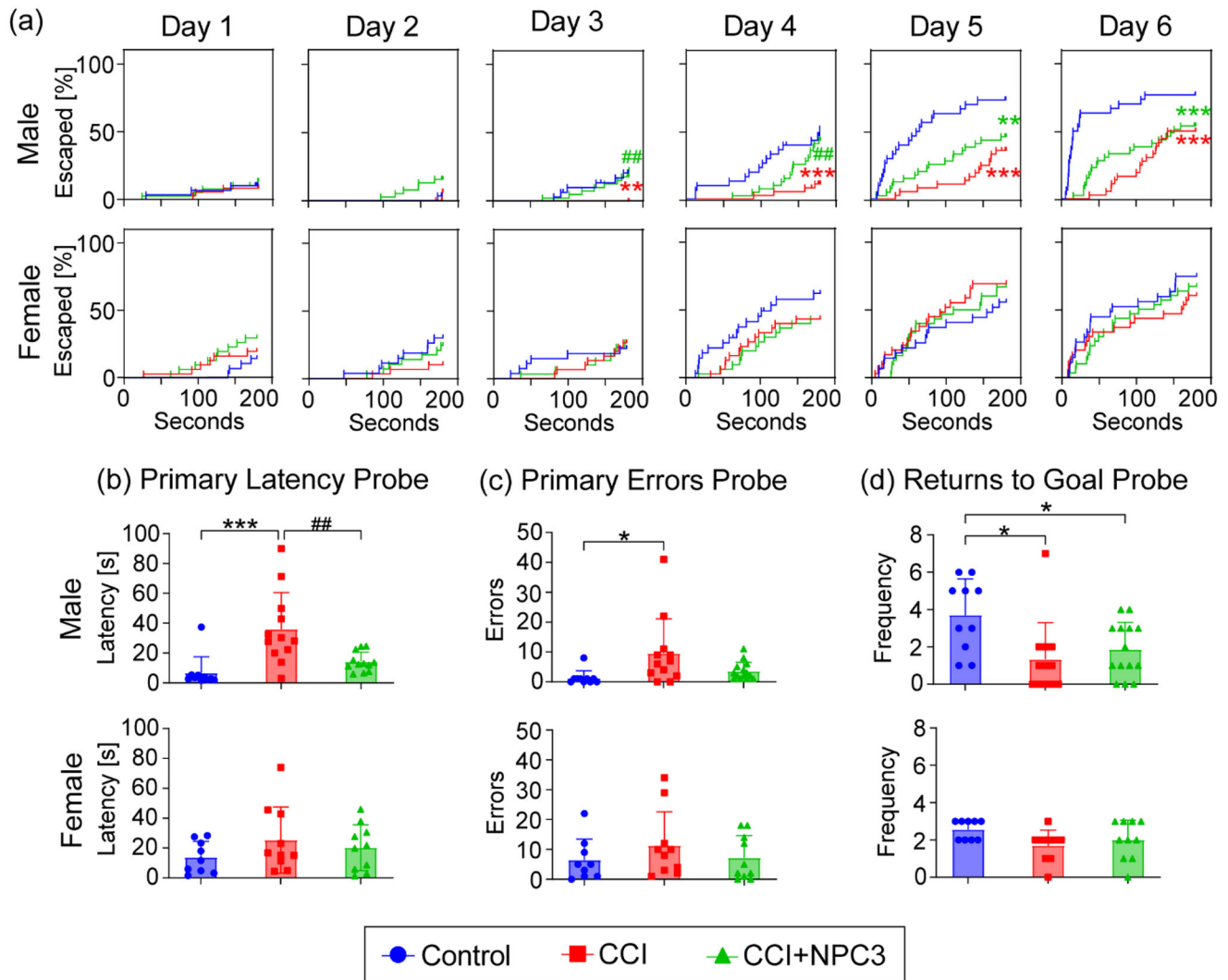


Figure 3. Barnes maze trials in male and female CCI mice to assess spatial learning and memory. a) Kaplan-Meier plots for escape frequency for male ($n = 30-42$) and female mice ($n = 27-30$). b–d) Probe trial data showing b) primary latency, c) primary errors, and d) returns to goal during the 90 s probe trial. Data are shown as mean \pm SD with $n = 10-14$ for male mice and $n = 9-10$ for female mice. * and # indicate a significant difference compared to the control group and the untreated CCI group, respectively, with one, two, and three symbols indicating $p < 0.05$, $p < 0.01$, and $p < 0.001$, respectively, as determined by Mantel-Cox method for the Kaplan-Meier plots, and one-way ANOVA for the primary latency, primary errors, and returns to goal on the probe day.

vein immediately following injury) to protect spatial learning and memory deficits caused by secondary injury following TBI. We found that the time for male CCI mice to escape the Barnes maze was significantly higher than the control mice starting from day 3 of Barnes maze trials, while the escape latency of NPC3 treated male CCI mice was significantly lower than the untreated CCI mice on day 3 and 4; the untreated male CCI mice caught up to the NPC3 treated CCI mice on day 5 and 6 (Figure 3A). In female mice, we did not find any significant difference between the escape latency of the control, untreated CCI mice, and NPC3 treated CCI mice on any day of the Barnes maze trials (Figure 3A). From search strategy analysis, we found that CCI reduced spatial learning and memory in male mice more significantly than in female mice (Figure 4). However, NPC3 treatment only improved the spatial search strategy on day 4 and probe trial in male mice,

and on day 3 in female mice. Thus, our results suggested that CCI affected spatial learning in male mice more than in female mice, as well as that NPC3 treatment protected the contralateral hippocampus in male CCI mice from secondary injury. On the probe trial day (Figure 3B,C,D), untreated male CCI mice performed worse than control mice in primary latency, primary errors, return to goal, as well as spatial search strategy (Figure 4). We did not find a significant difference between the control and NPC3 treated male CCI mice, except that NPC3 treated male CCI mice had significantly less return to goal than control mice. We found that the NPC3 treated male CCI mice had a significant reduction in primary latency, as well as a trending improvement in the primary error, return to goal, and spatial search strategy, compared to the untreated CCI mice. For female mice, the primary latency, primary errors, and total errors of the control, NPC3

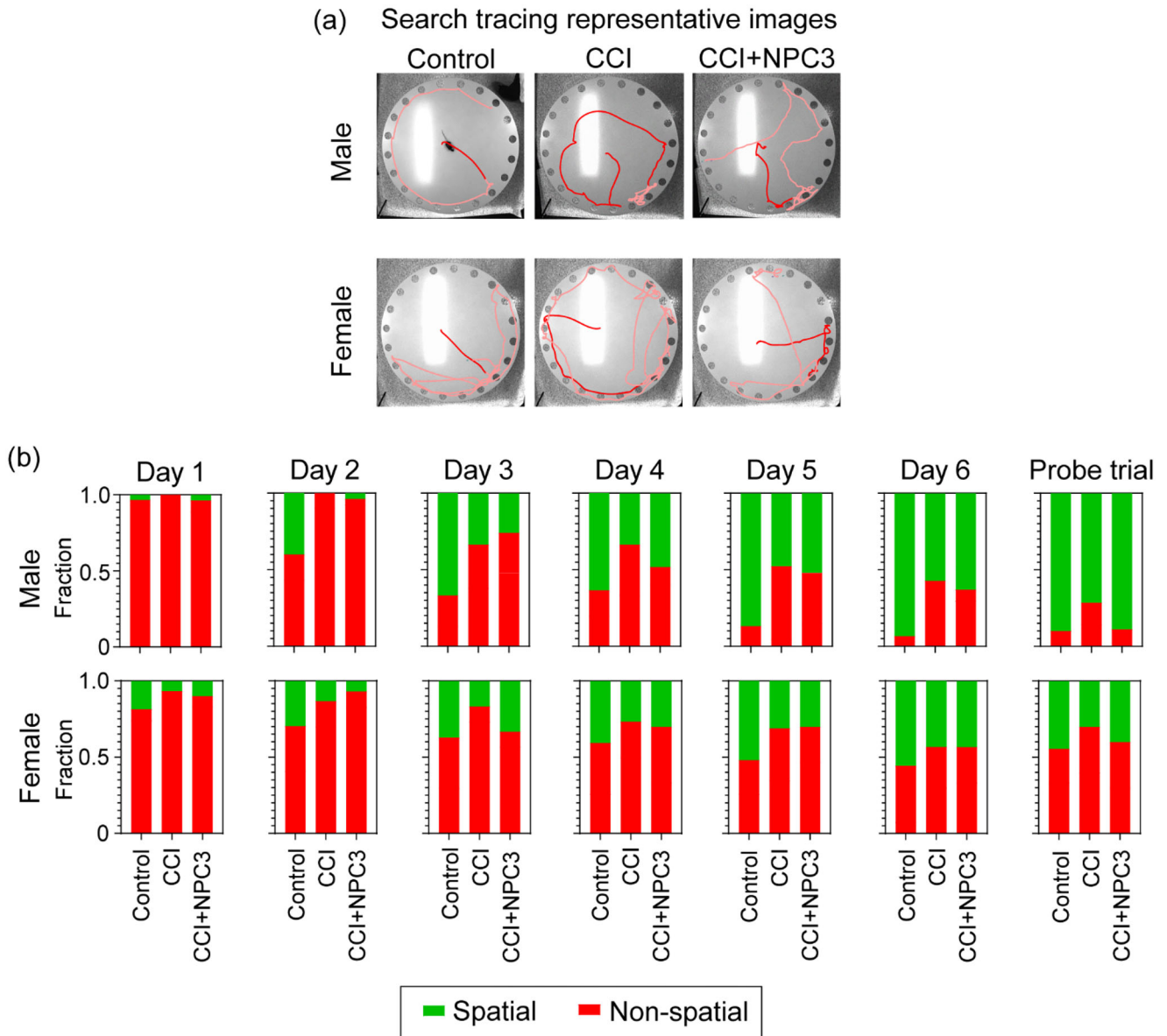


Figure 4. The search strategy of Barnes maze trials in male and female mice. a) Representative search tracing on probe trial day with bright red showing the trace to the escape box and opaque red showing the trace until reaching 90 s. b) Classification of spatial and non-spatial search strategy in male and female mice on day 1–6 ($n = 30$ – 42 for males and $n = 27$ – 30 for females) and probe trial ($n = 10$ – 14 for males and $n = 9$ – 10 for females) day of Barnes maze trials.

treated, and untreated female CCI mice were similar throughout the trials. Thus, further suggests that the NPC3 treatment protected the contralateral hippocampus in male CCI mice from secondary injury, while female CCI mice benefited less from the antioxidant treatment of NPC3 to protect the contralateral hippocampus from secondary injury.

2.4. Time Course of Carbonyl Stress in Male and Female Mice Following TBI

To identify possible molecular mechanisms for differences in spatial learning and memory deficits following CCI in male and

female mice (Figure 3) despite similar NPC3 accumulation kinetics (Figure 1) and reduction in oxidative stress (Figure 2), we investigated the reduction of the spread of carbonyl stress following injury. We utilized Western blotting (Figure 5 and 6) to measure 4-hydroxynonenal (4-HNE)- and acrolein-modified proteins, two of the most prevalent LPOx following TBI,^[15] at 1, 3, and 7 d post-injury when carbonyl stress is most elevated.^[16]

At 1 d post-injury, we found a significant increase in 4-HNE (Figure 5A2 and Figure 6A2) and acrolein (Figure 5A4 and 6A2) in the ipsilateral cortex and hippocampus of the untreated male CCI mice, as well as a trending increase in the untreated female CCI mice (Figure 5B2, 5B4, 6B2, and 6B4). At 1 d post-injury, we also found a trending increase in acrolein in the

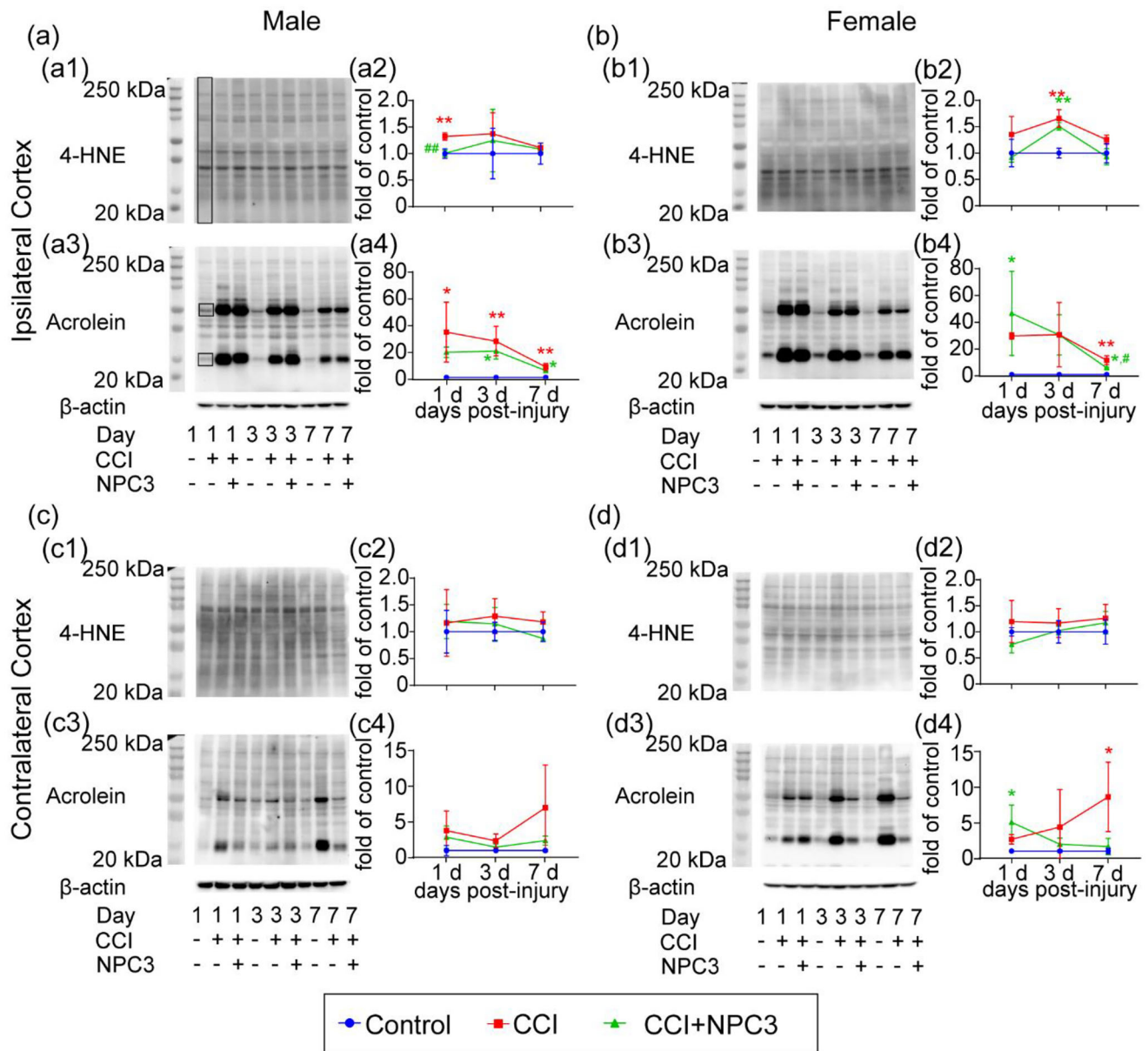


Figure 5. Analysis of carbonyl stress in the cortex. Western blot analysis of LPOx 4-HNE and acrolein in the ipsilateral a,b) and contralateral c,d) cortex for male a,c) and female b,d) mice at 1, 3, and 7 d post-injury. a1,b1,c1,d1) Representative blots of 4-HNE in the ipsilateral and contralateral cortex. The boxed area represents the region of interest (ROI) used for quantification. a3,b3,c3,d3) Representative blots of acrolein in the ipsilateral and contralateral cortex. The boxed area represents the ROI for quantification. a2,b2,c2,d2) Quantification of 4-HNE in the ipsilateral and contralateral cortex normalized to β -actin. a4,b4,c4,d4) Quantification of acrolein in the ipsilateral and contralateral cortex normalized to β -actin. Data are shown as mean \pm SD with $n = 3$ for each treatment group. * and # indicate a significant increase compared to the control group and a significant decrease compared to the untreated CCI group, respectively, with one, two, and three symbols indicating $p < 0.05$, $p < 0.01$, and $p < 0.001$, respectively, as determined by one-way ANOVA and Tukey's post hoc test.

contralateral cortex (Figure 5C4) and hippocampus (Figure 6C4) of male CCI mice. At 3 d post-injury, we found a significant increase in acrolein (Figure 5A4) and 4-HNE (Figure 6A2) in the ipsilateral cortex and hippocampus of the untreated male CCI mice, respectively, as well as 4-HNE in the ipsilateral cortex (Figure 5B2) and hippocampus (Figure 6B2) of the untreated female CCI mice. At 3 d post-injury, we also observed a trending increase in 4-HNE (Figure 5A2) and acrolein (Figure 6A4)

in the ipsilateral cortex and hippocampus of male CCI mice, respectively, and acrolein in the ipsilateral cortex (Figure 5B4) and hippocampus (Figure 6B4) of female CCI mice. At 7 d post-injury, we found a significant increase in acrolein in the ipsilateral cortex (Figure 5A4) and hippocampus (Figure 6A4) of the untreated male CCI mice, and the ipsilateral cortex of the untreated female CCI mice (Figure 5B4). At 7 d post-injury, we also found a trending and significant increase in acrolein in the contralateral cortex

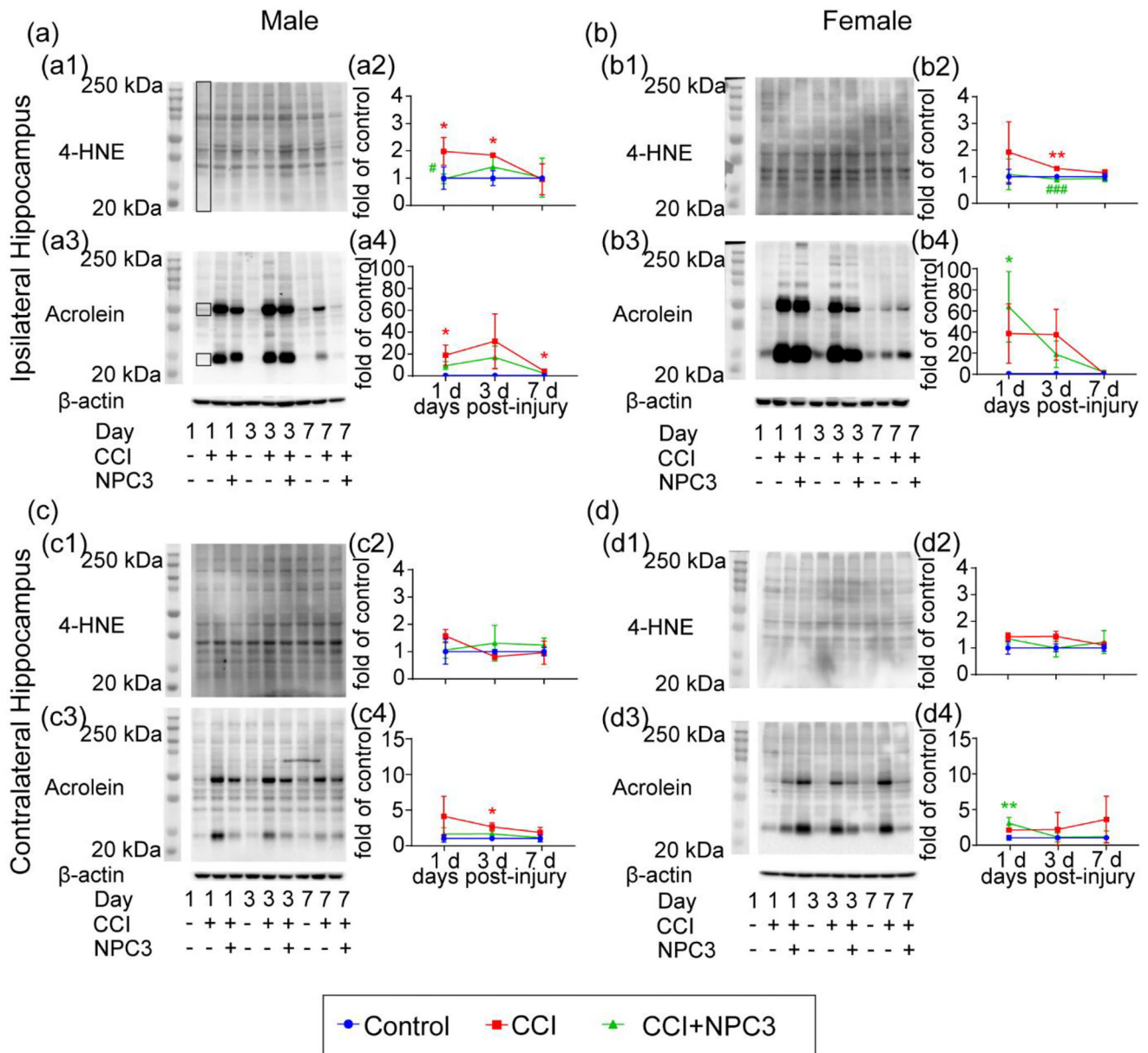


Figure 6. Analysis of carbonyl stress in the hippocampus. Western blot analysis of 4-HNE and acrolein in the ipsilateral a,b) and contralateral c,d) hippocampus for male a,c) and female b,d) mice at 1, 3, and 7 d post-injury. a1,b1,c1,d1) Representative blots of 4-HNE in the ipsilateral and contralateral hippocampus. The boxed area represents the ROI for quantification. a3,b3,c3,d3) Representative blots of acrolein in the ipsilateral and contralateral hippocampus. The boxed area represents the ROI for quantification. a2,b2,c2,d2) Quantification of 4-HNE in the ipsilateral and contralateral hippocampus normalized to β -actin. a4,b4,c4,d4) Quantification of acrolein in the ipsilateral and contralateral hippocampus normalized to β -actin. Data are shown as mean \pm SD with $n = 3$ for each treatment group. * and # indicate a significant increase compared to the control group and a significant decrease compared to the untreated CCI group, respectively, with one, two, and three symbols indicating $p < 0.05$, $p < 0.01$, and $p < 0.001$, respectively, as determined by one-way ANOVA and Tukey's post hoc test.

of male (Figure 5C4) and female (Figure 5D4) CCI mice, respectively, as well as a trending increase in acrolein in the contralateral hippocampus of female CCI mice (Figure 6D4).

We observed a significant and trending reduction in 4-HNE with NPC3 treatment at 1 d post-injury in male (Figure 5A2 and 6A2) and female mice (Figure 5B2 and 6B2), respectively, in the ipsilateral cortex and hippocampus. At 3 d post-injury, we observed a trending and significant reduction in 4-HNE

with NPC3 treatment in male (Figure 6A2) and female mice (Figure 6B2), respectively, in the ipsilateral hippocampus. We also observed a trending reduction in acrolein with NPC3 treatment at 7 d post-injury in the contralateral cortex of male mice (Figure 5C4) and contralateral cortex (Figure 5D4) and hippocampus (Figure 6D4) of female mice, as well as a significant reduction in acrolein in the ipsilateral cortex of female mice (Figure 6B4).

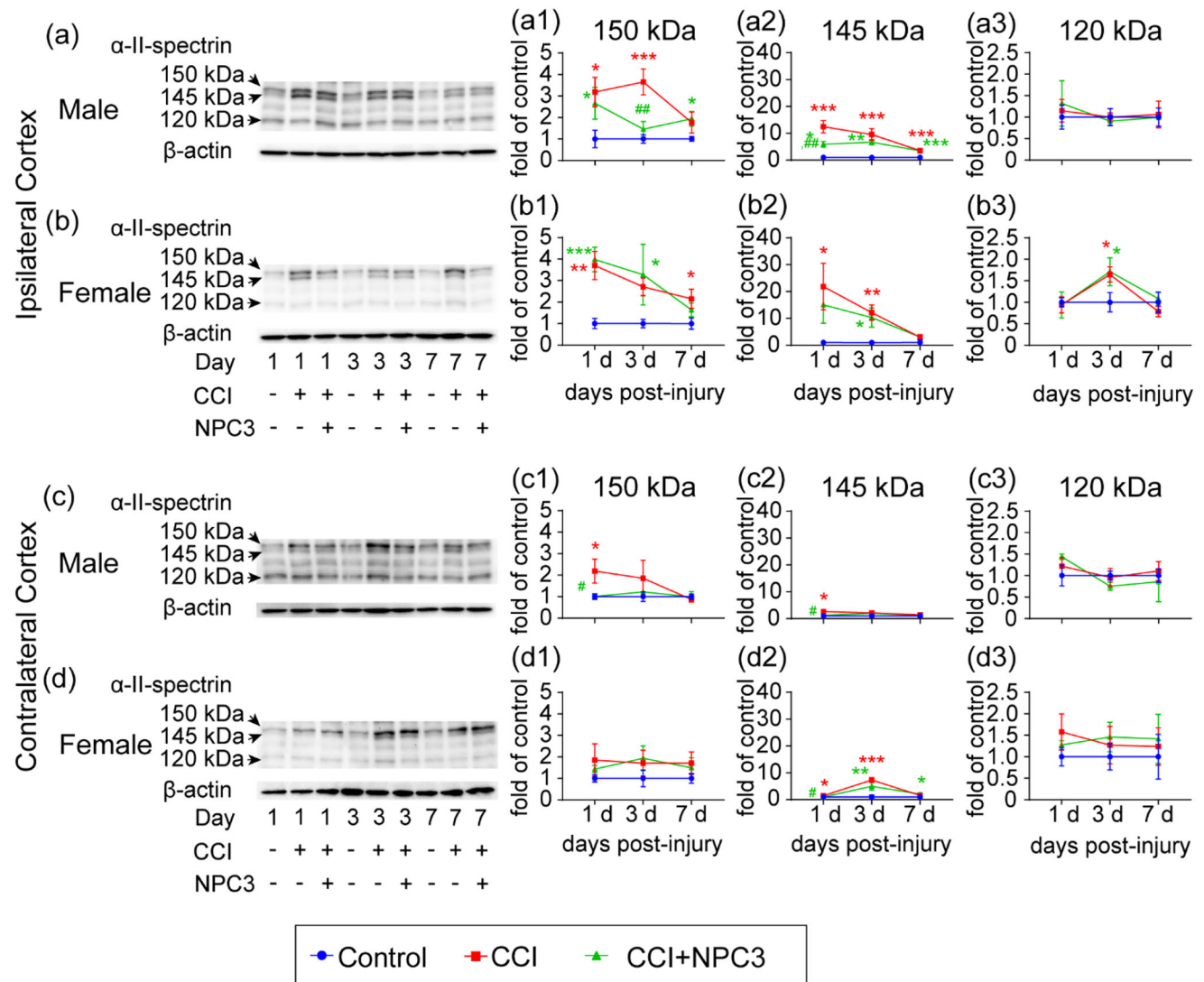


Figure 7. Analysis of SBDPs in the cortex. Western blot analysis of SBDPs in the ipsilateral a,b) and contralateral c,d) cortex for male a,c) and female (b,d) mice at 1, 3, and 7 d post-injury. a,b,c,d) Representative blots of SBDPs in the ipsilateral and contralateral cortex. Quantification of 150 kDa SBDP (proportional to total cell death) a1,b1,c1,d1), 145 kDa SBDP (proportional to necrosis) a2,b2,c2,d2), and 120 kDa SBDP (proportional to apoptosis) a3,b3,c3,d3) normalized to β -actin, respectively. Data are shown as mean \pm SD with $n = 3$ for each treatment group. * and # indicate a significant increase compared to the control group and a significant decrease compared to the untreated CCI group, respectively, with one, two, and three symbols indicating $p < 0.05$, $p < 0.01$, and $p < 0.001$, respectively, as determined by one-way ANOVA and Tukey's post hoc test.

2.5. Time Course of α -II-Spectrin Degradation in Male and Female Mice Following TBI

Finding that NPC3 treatment significantly reduced ROS but did not have a notable effect on the spread of LPOx to the contralateral hemisphere following brain injury, we investigated if there were differences in cell death following brain injury. We analyzed cell death through the necrosis and apoptosis pathways through Western blotting of α -II-spectrin breakdown products (SBDPs) to identify apoptosis (caspase degradation pathway, 120 kDa), necrosis (calpain degradation pathway, 145 kDa), and total cell death (caspase and calpain degradation pathways, 150 kDa) (Figure 7 and 8).^[17] We chose 1, 3, and 7 d post-injury to measure SB-

DPs when SBDPs are most elevated in the subacute phase of the injury.^[16]

We found significant and trending increases in 150 and 145 kDa SBDPs at 1, 3, and 7 d post-injury in the ipsilateral cortex and hippocampus of the untreated male and female CCI mice, except the 145 kDa SBDP in the ipsilateral cortex (Figure 7B2) and 150 (Figure 8B1) and 145 kDa SBDPs (Figure 8B2) in the ipsilateral hippocampus of the untreated female CCI mice at 7 d post-injury. At 1 d post-injury, we also observed a significant increase in 150 (Figure 7C1) and 145 kDa SBDPs (Figure 7C2) in the contralateral cortex, as well as a trending increase in 145 kDa SBDP (Figure 8C2) in the contralateral hippocampus, of the untreated male CCI mice. We observed a significant increase in 145 kDa

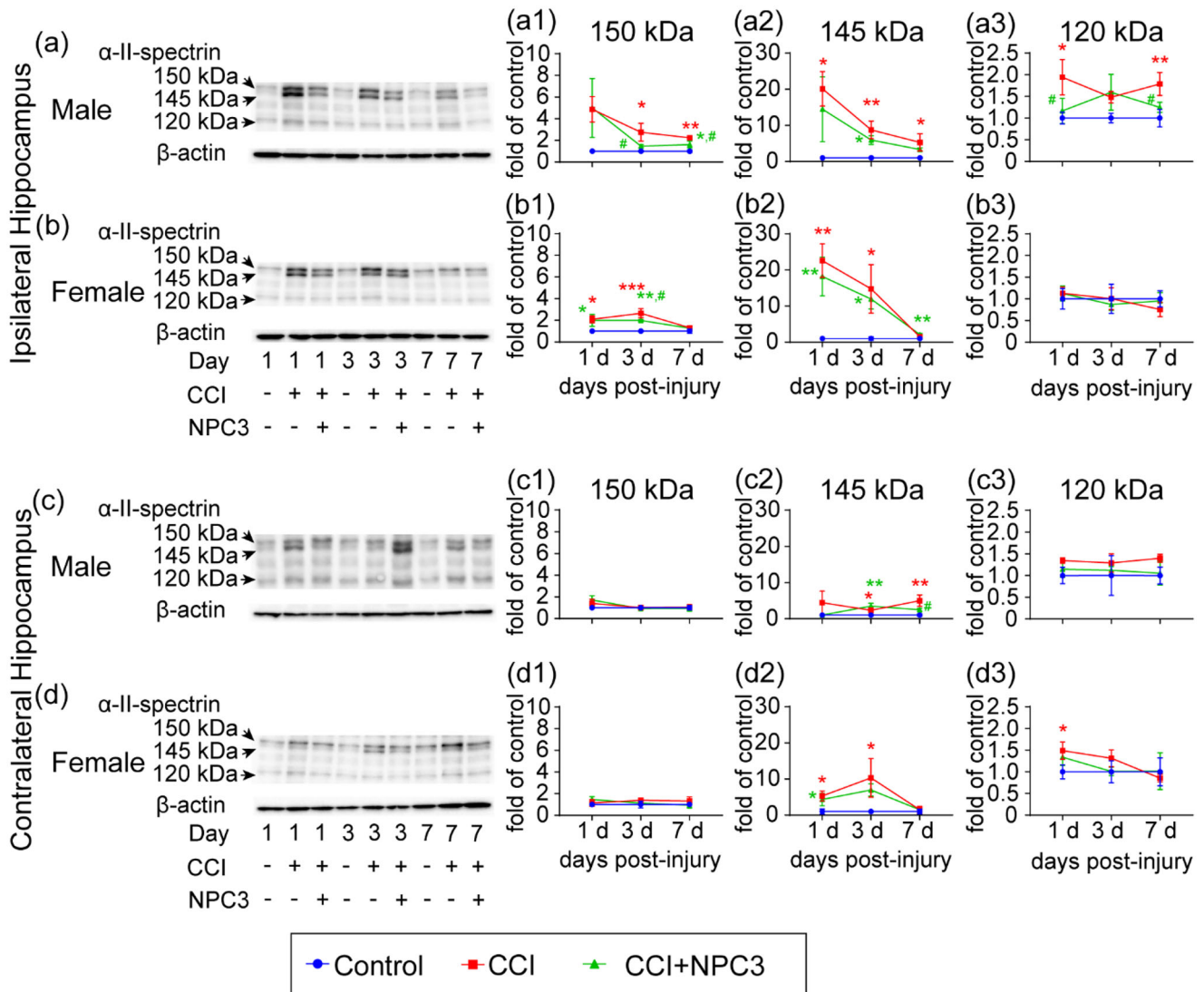


Figure 8. Analysis of SBDPs in the hippocampus. Western blot analysis of SBDPs in ipsilateral a,b) and contralateral c,d) hippocampus for male a,c) and female b,d) mice at 1, 3, and 7 d post-injury. a,b,c,d) Representative blots of SBDPs in the ipsilateral and contralateral cortex. Quantification of 150 kDa SBDP (proportional to total cell death) a1,b1,c1,d1), 145 kDa SBDP (proportional to necrosis) a2,b2,c2,d2), and 120 kDa SBDP (proportional to apoptosis) a3,b3,c3,d3) normalized to β -actin, respectively. Data are shown as mean \pm SD with $n = 3$ for each treatment group. * and # indicate a significant increase compared to the control group and a significant decrease compared to the untreated CCI group, respectively, with one, two, and three symbols indicating $p < 0.05$, $p < 0.01$, and $p < 0.001$, respectively, as determined by one-way ANOVA and Tukey's post hoc test.

SBDP in the contralateral cortex (Figure 7D2) and hippocampus (Figure 8D2) of female CCI mice at 1 and 3 d post-injury. Most notably, we observed bilateral necrotic cell death (145 kDa SPDP) at 7 d post-injury in the hippocampus of male CCI mice that was protected by NPC3 treatment (Figure 8A2 and 8C2). This bilateral necrotic cell death was not apparent in the hippocampus of CCI or NPC3 treated female mice (Figure 8B2 and 8D2). For the caspase-3 apoptosis pathway (120 kDa), we did not observe significant changes, except in the ipsilateral cortex of female mice at 3 d post-injury (Figure 7C3), the ipsilateral hippocampus of male mice at 1 and 7 d post-injury (Figure 8A3), and contralateral hippocampus of female mice at 1 d post-injury (Figure 8D3).

We did not observe any significant reduction in 150 kDa SBDP with NPC3 treatment in the ipsilateral cortex (Figure 7B1) and

hippocampus (Figure 8B1) of female mice, except in the ipsilateral hippocampus at 3 d post-injury, compared to the untreated female CCI mice. We observed a significant decrease in 150 kDa SBDP in the ipsilateral cortex (Figure 7A1) and hippocampus (Figure 8A1) of the NPC3 treated male CCI mice at 3 d post-injury, and in the ipsilateral hippocampus at 7 d post-injury, compared to the untreated male CCI mice. We also observed a significant decrease in 145 kDa SBDP with NPC3 treatment in the ipsilateral cortex at 1 d post-injury in male mice (Figure 7A1). In the contralateral cortex, we observed a significant reduction in 150 (Figure 7C1) and 145 kDa SBDPs (Figure 7C2) at 1 d post-injury in the NPC3 treated male mice, and 145 kDa SBDP at 1 d post-injury in the NPC3 treated female mice (Figure 7D2), compared to the untreated male and female CCI mice. We also observed

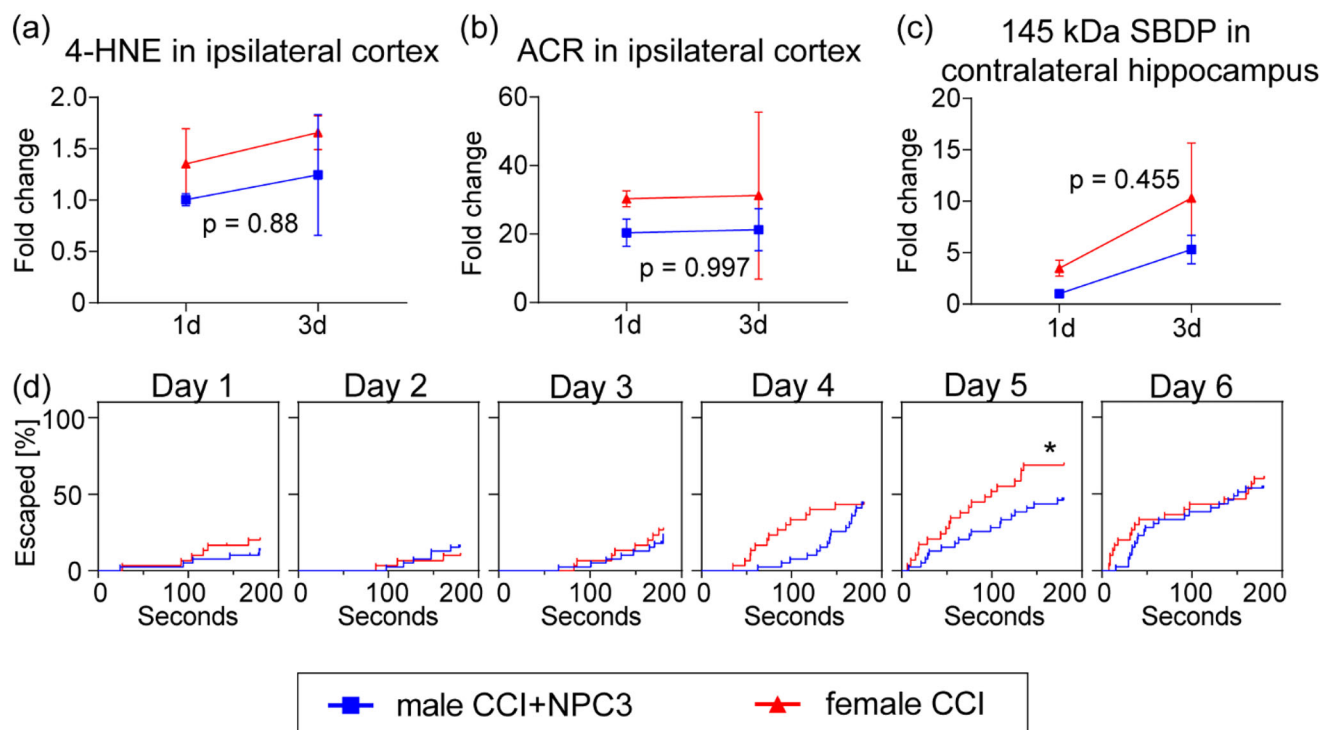


Figure 9. Comparison between NPC3 treated male CCI mice and untreated female CCI mice. The slope of NPC3 treated male CCI mice (blue) and untreated female CCI mice (red) for a) 4-HNE and b) acrolein in the ipsilateral cortex, as well as c) necrosis in the contralateral hippocampus, were not significantly different, as determined by simple linear regression comparison analysis. d) There is not any significant difference between the NPC3 treated male mice and untreated female mice in latency to escape the Barnes maze, except on day 5 ($p < 0.05$), as determined by Mantel-Cox.

a trending and significant decrease in 145 kDa SBDP at 1 and 7 d post-injury, respectively, in the contralateral hippocampus of the NPC3 treated male CCI mice compared to the untreated male CCI mice (Figure 8C2). At 3 d post-injury, a slight reduction in 145 kDa SBDP was observed in the contralateral cortex (Figure 7D2) and hippocampus (Figure 8D2) of the NPC3 treated female CCI mice compared to the untreated female CCI mice. We did not observe significant changes in 120 kDa SBDP with NPC3 treatment compared to the untreated male and female CCI mice, except in the ipsilateral hippocampus of male mice at 1 and 7 d post-injury (Figure 8A3).

2.6. Oxidative Stress Markers and Spatial Learning Comparison Between NPC3 Treated Male CCI Mice and Untreated Female CCI Mice

From the Western blot of LPOx and SBDPs, we found that NPC3 treatment reduced the spread of carbonyl stress in the ipsilateral cortex, as well as total cell death and necrosis into the contralateral hippocampus in the male CCI mice, while female mice did not show significant benefit from the NPC3 treatment. Our CCI is performed on the left frontoparietal cortex since spatial learning and memory is more heavily on the right hippocampus in mice,^[18] thus there must be secondary spread of injury to the right hippocampus to have the most significant effects on spatial learning and memory. Therefore, neuroprotection of the con-

tralateral hippocampus with NPC3 treatment would result in the improvement of spatial learning and memory in CCI mice.

Finding the similarity of the changes in LPOx and SBDPs between NPC3 treated male and untreated female CCI mice, we statistically tested the similarity of the slopes between NPC3 treated male CCI mice and untreated female mice for 4-HNE and acrolein in the ipsilateral cortex, and 145 kDa SBDP in the contralateral hippocampus (Figure 9A–C). We found that the trend in time-course of LPOx and SBDP is more similar between NPC3 treated male CCI mice and untreated female CCI mice than between NPC3 treated and untreated male CCI mice (Figure S3A, Supporting Information), as well as between untreated male and female CCI mice (Figure S3B, Supporting Information).

We also compared the survival curve between NPC3 treated male CCI mice and untreated female CCI mice (Figure 9D). We found that the NPC3 treated male CCI mice performed similarly to the untreated female CCI mice. On the other hand, untreated female CCI mice performed significantly better than the untreated male CCI mice on days 3 to 5, as well as slightly better on the other days (Figure S3C, Supporting Information).

From comparing the time-course of LPOx and SBDP, as well as the survival curve, of NPC3 treated male CCI mice and untreated female mice, our results suggest that female mice might have enough endogenous antioxidant activities to prevent the spread of secondary injury.^[19] On the other hand, male mice need additional oxidative stress scavengers through NPC3 treatment.

3. Discussion

Following a TBI, elevated production of ROS oxidizes cell membranes and fatty acids producing LPOx. LPOx then exacerbates injury progression by oxidizing other lipids and proteins. Therefore, there is a need for ROS and LPOx scavengers to reduce the progression of TBI. Theranostic neuroprotective copolymers (NPC3) with thiol functional groups showed scavenging activity against both H₂O₂ and LPOx (Table 1).^[9] Thiol functional groups are also known to react with peroxynitrite and nitric oxide.^[20] Thus, NPC3 expands the scavenging activity compared to our previous thioether ROS scavengers.^[2b,13]

A treatment window, also known as a therapeutic time window, is defined as a period of time that a treatment can successfully engage with a therapeutic target. The treatment window identified for antioxidant therapies for TBI that have entered clinical trials is around 4 h post-injury.^[21] One of the limiting factors of the treatment window in clinical trials might be the decrease in accumulation of small molecule drugs in the injured brain when administered later than 4 h post-injury.^[8b,22] Here, we found that the accumulation of NPC3 (Figure 1) was the highest when administered immediately following the injury, and significantly reduced when administered starting at 3 h post-injury in females, and 6 h post-injury in males, corroborating previous studies.^[7a,8b,8c,8k] The treatment window of 9 nm NPC3, which was up to 6 h post-injury in male mice, was longer than the treatment window of 20, 40, 100, and 500 nm PEGylated-NPs, which were less than 2 h post-injury.^[8c] Overall, this finding corroborated that the size of NPs is essential in determining the accumulation of NPs in the brain lesion. This finding also suggests that smaller NPs may extend the therapeutic time window for antioxidant TBI treatment. However, NPC3 might need to be functionalized with targeting ligands, such as CAQK peptide, to improve the accumulation in the lesion when administered at more than 4 h post-injury;^[23] the time that almost 50% of the TBI patients arrived at the hospital.^[24]

The therapeutic window is essential in antioxidant treatments due to the bell-shaped response curve of antioxidant treatment in TBI.^[14c,14e,14f] in which suboptimal dosing of antioxidants would give a suboptimal reduction in oxidative stress or even exacerbate the injury progression.^[10,14a-e] Here, we found the therapeutic window of NPC3 was between 2.1–20.8 mg kg⁻¹ NPC3 for male CCI mice and 5.5–27.6 mg kg⁻¹ NPC3 for female CCI mice. Since the therapeutic windows of males and females were studied separately (Figure 2B), the difference in dose between sexes should not act as a confounding variable in this study since both doses were within the middle of their respective therapeutic windows. Comparing NPC3 to our previous study with NP1,^[2b] 0.2 mg mouse⁻¹ NPC3 only scavenges ≈5% of the total ROS levels that was scavenged by 0.1 mg mouse⁻¹ NP1, but we observed a similar reduction in oxidative stress with NPC3 treatment (68% reduction in males and 58% reduction in females) compared to NP1 treatment (68% reduction in females). This is likely a result of the nearly immediate reaction rate of NPC3 with ROS whereas NP1 does not fully react until hours following exposure to ROS. Furthermore, the multiple scavenging activities of thiol groups on NPC3 to bind with ROS, reactive nitrogen species, lipid radicals, and LPOx, might be more effective in mitigating the secondary injury cascade compared to ROS-only scavengers

with thioether bonds in NP1. In addition, oxidized thiol groups on NPC3 may also be reduced by glutathione and glutathione reductase, and reused, which translates to a higher scavenging activity of NPC3 in vivo than the theoretical number from HRPO assay.^[9] Since we administered NPC3 immediately following injury, the reduction in ROS at 4 h post-injury was likely primarily due to the ROS scavenging of NPC3 since LPOx do not peak until around 3 d post-injury.^[16,25]

To test if NPC3 dosed within its treatment and therapeutic window to CCI mice can protect CCI-mediated spatial learning and memory deficits, we performed Barnes maze analysis at 1 month post-injury in the chronic phase of the injury. We perform our CCI over the left frontoparietal cortex to limit primary damage to the right hippocampus that plays an essential role in spatial learning and memory.^[2b,18] Thus, the most significant deficits in spatial learning and memory would be caused by secondary spread of injury to the contralateral hippocampus in our model, resulting in bilateral hippocampal dysfunction. We found that the untreated male CCI mice learned to escape the maze slower than the control and NPC3 treated mice (Figure 3A). Similar to previous studies,^[2b,26] untreated male CCI mice showed a non-spatial search strategy preference in escaping the maze (Figure 4). However, control and NPC3 treated male mice utilized more spatial search strategies as indicated by shorter primary latencies, fewer primary errors, and more returns to goal during the probe trial as compared to male CCI mice (Figure 3B–D).^[27] On the other hand, in female mice we did not find spatial learning and memory deficits from severe CCI. This suggests there is likely important sex-based differences in the bilateral spread of secondary injury in the hippocampus in CCI mice, and thus by extension, differences in the therapeutic efficacy of NPC3 and other antioxidant treatments. These results find support from our previous findings with NP1 treatment on a milder CCI mouse model of TBI, in which male, but not female, CCI mice showed spatial learning and memory deficits compared to the NP1 treated mice and control mice (supplementary data of ref^[2b]). Furthermore, clinically, tirilazad was found to only provide a significant therapeutic benefit in male TBI patients with traumatic subarachnoid hemorrhage, but not in females, which suggests there may be clinical relevance to our findings.^[28]

To compare the bilateral spread of secondary injury biomarkers in the hippocampus between male and female mice, we tracked LPOx levels and mechanisms of cell death through the sub-acute phase of the injury. 4-HNE and acrolein are two of the most abundant and reactive LPOx aldehydes, and readily form covalent bonds with cysteine of proteins.^[15] Since we found a reduction in ROS with NPC3 treatment in the acute phase of injury, we expected to see a reduction in LPOx in the subacute phase of injury, as found in previous studies.^[2b,14a,14c,14e,29] Here, we found reductions of 4-HNE with NPC3 treatment at 1 d post-injury in the ipsilateral cortex and hippocampus of male and female mice (Figure 5A and 6A). However, there were no notable differences in LPOx between treatment groups at other time points (Figures 5–6). Similarly, although we found a trending reduction of acrolein in the contralateral cortex and hippocampus in male and female mice, there were no notable differences in LPOx between treatment groups. This may suggest that LPOx do not play a predominant role in the spread of secondary injury, or LPOx

level changes following TBI may be lower than our study was statistically powered for.

Following a TBI, excess production of ROS increases Ca^{2+} influx into mitochondria. Ca^{2+} also activates the calpain and caspase-3 enzymes that drive necrosis and apoptosis cell death pathways, respectively, as well as degrade α -II-spectrin in two different pathways. In the ipsilateral hemisphere, SBDPs peaked at 1 d post-injury in the NPC3 treated and untreated male and female CCI mice (Figures 7–8). Most notably, we observed the bilateral spread of necrotic cell death in the hippocampus late in the sub-acute phase of the injury (day 7) in male CCI mice (Figure 8C2). This bilateral spread of necrosis was not observed in male CCI mice treated with NPC3 suggesting protection from this secondary injury. Interestingly, we did not observe a bilateral spread of necrosis in female CCI mice. The minimal changes in 120 kDa SBDP compared to 150 and 145 kDa SBDPs also suggested that necrosis dominates the cell death pathways in severe CCI mouse model of TBI.^[30] These data combined with our behavioral findings suggest that this spread of necrotic, but not apoptosis, cell death bilaterally in the hippocampus contributes to spatial learning and memory deficits. We did not observe this bilateral spread of necrosis in female mice, which may stem from higher glutathione,^[19b] glutathione-S-transferase,^[19c] and catalase^[19a,19d] activities in the brain of females as compared to males, which may provide protection from CCI-induced excessive oxidative stress and necrotic cell death. NPC3 treatment in male mice prevented the bilateral spread of necrosis within the hippocampus and resulted in reduced spatial learning and memory deficits similar to that observed in female CCI mice (Figure 9). Of note, NPC3 treated female CCI mice did not perform better than female CCI mice suggesting NPC3 treatment did not provide any additional therapeutic benefit above the natively higher antioxidant expression levels^[19] in female brain. This, combined with our recent work with antioxidant enzyme loaded NPs in male and female mice,^[10] strongly suggest there is a threshold of total antioxidant activity in the brain following CCI, above which no additional therapeutic benefit is observed. This underscores the importance of the need for multiple therapeutic targets to improve therapeutic efficacy following TBI.

A possible limitation of this study is that we did not synchronize and monitor estrous in female mice. However, there appears to be minimal correlation between the estrous cycle and TBI outcomes,^[31] indicating synchronization of estrous may not be needed. Indeed, our results also showed similar individual variabilities in males and females, especially in the subacute phase of injury. However, progesterone and estrogen are known to play roles in neuroprotection and antioxidant activities.^[32] All of the 0 mg kg^{-1} female mice and two of the 5.5 mg kg^{-1} female mice came from the same cohort and confinement, and thus there is a possibility that 5 out of 6 unsynchronized female mice were in the same stage of the estrous cycle.^[33] Therefore, there is a possibility that they were all in the estrus stage at the time of the injury, when progesterone and estrogen were at their lowest, which may lead to a higher increase in oxidative stress compared to the untreated male mice. It is also a possibility that the sex-based differences we observed in this study were caused by size differences between males and females. However, we employed robust analysis methods, which are not sensitive to size differences, such as K^{trans} , to identify the treatment and therapeutic windows of

male and female CCI mice individually and dosed males and females accordingly based on these results. Therefore, we strongly believe that our results are not confounded by size differences between sexes. Another limitation of this study is the sample size for the animal experiments, which may not be sufficiently powered to detect important differences between male and female mice. Sufficiently powering the time-course studies looking at bilateral necrosis would require a very large number of additional animals, so it is beyond the scope of this work. However, our data point to the importance of sex on TBI outcomes with antioxidant NP treatment and highlight the need for future studies in this area, especially correlating bilateral spread of injury at the sub-acute phase of injury with functional outcomes.

4. Conclusion

The secondary spread of elevated free radical levels, LPOx, and cell death following a TBI has prevented the development of an effective therapy that has shown efficacy in Phase III clinical trials. Our long-term goal is to utilize NP technologies to help reduce secondary injury progression following TBI. To this end, an ROS and LPOx scavenger NP (NPC3) was developed that contained thiol functional groups that provide rapid sequestration of both ROS and LPOx. In this study, we established the treatment and therapeutic windows of NPC3 in male and female CCI mice to establish an optimal dosing scheme to compare treatment efficacies. We found maximal accumulation of NPC3 when injected immediately following injury in both males and females, with a treatment window out to 3 h post-injury and marked drop-off 6 h post-injury. We found therapeutic windows for reduction in oxidative stress of 2.1–20.8 mg kg^{-1} NPC3 in males and 5.5–27.6 mg kg^{-1} in females. NPC3 treatment for CCI mice within these therapeutic windows resulted in protection of spatial learning and memory deficits in male mice more than female CCI mice. We found that NPC3 treatment was required in male mice to protect from the bilateral spread of necrosis in the hippocampus whereas the untreated female CCI mice did not show this bilateral spread. Therefore, bilateral hippocampal necrosis, which NPC3 treatment was able to protect from, seems to contribute to the spatial learning and memory deficits observed following CCI in mice. Overall, this signifies some sex-based differences in the spread of secondary injury following TBI, and suggest an upper threshold of antioxidant activity that provides neuroprotection beyond which no additional therapeutic benefit is seen since female mice benefit less from NPC3 treatment than male mice.

5. Experimental Section

Neuroprotective Copolymers (NPC3) Synthesis: 20 wt.% LIPOMA polymer (NPC3) were synthesized as previously described.^[9] Briefly, poly(ethylene glycol) methyl ether methacrylate monomer (O950; 4.00 g, 4.21 mmol), lipoic acid methacrylate monomer (LIPOMA; 1.00 g, 3.10 mmol), 3.59 mL of a 25 mg mL^{-1} of 4-(((2-carboxyethyl)thio)carbonothioyl)thio)-4-cyanopentanoic acid (CCC) stock in dimethylacetamide (DMAc; 90 mg, 0.293 mmol), 410 μL of a 10 mg mL^{-1} 4,4'-azobis (4-cyanovaleric acid) (ABCVA) in dimethyl sulfoxide (DMSO) (4.1 mg, 0.015 mmol), DMAc (3.5 g), and 1.15 g of sodium borohydride (NaBH_4 ; 31 mmol, 10:1 M ratio) were reacted under argon gas at 70 °C for 24 h. The polymers were dialyzed in Spectrapor

regenerated cellulose dialysis membrane against ethanol for one day followed by deionized (DI) water for two days, before they were freeze-dried. Quality control for NPC3 was a hydrodynamic size of 9 nm and scavenging ability of around 0.25 $\mu\text{mol ROS}$ and 0.07 $\mu\text{mol LPOx}$ per mg NPC3.

Gadolinium-conjugated NPC3 (NPC3-Gd) was synthesized by adding gadolinium-tetraazacyclododecanetetraacetic acid methacrylate monomer (GdMA; 121 mg, 0.217 mmol) to NPC3 (1 g, 0.058 mmol in CCC), ABCVA (100 μL of a 16.09 mg mL^{-1} stock in ethanol), O950 (0.22 g, 0.232 mmol), and DI water (4.15 mL). NPC3-Gd was only utilized for DCE-MRI and did not have antioxidant capacity since NPC3-Gd was not reduced with NaBH_4 .

Controlled Cortical Impact Mouse Model of TBI: All animal procedures were performed in accordance with approval by the University of Nebraska–Lincoln IACUC (protocol number 2300). The controlled cortical impact (CCI) mouse model of TBI was performed as described previously with some modifications.^[9] Briefly, 8- to 10-week-old male and female C57BL/6 mice (Jackson Laboratory, Bar Harbor, ME, USA) were acclimated for at least three days prior to the procedures. During the CCI, mice were fully anesthetized through isoflurane inhalation. A midline incision was made to expose the skull and a craniectomy performed using a 2.5-mm trephine drill to expose an intact dura. An impact normal to dura was performed using a 2-mm convex tip over the left frontoparietal cortex (2 mm anterior and 2 mm left of lambda). The impact parameters were 2.5 mm depth, 4 m s^{-1} velocity, and 80 ms dwell time. Tissue adhesive was administered on the scalp to seal the incision following the CCI.

Estrous in female mice was not regulated at the time of injury since estrous cycle stages at the time of the injury has little effect on neuroprotection in female rodents.^[31a,31b] The variability of the secondary injury markers were also similar between male and female mice with both controlled and randomized estrous cycle at the time of injury.^[31]

In vivo Dynamic Contrast-Enhanced Magnetic Resonance Imaging (DCE-MRI)

In vivo NP assessment consisted of dynamic contrast-enhanced (DCE)-MRI was taken with a 9.4T MRI system (Varian). The MRI system was equipped with a 4-cm Millipede RF imaging probe with triple-axis gradients (100 G cm^{-1} max). DCE-MRI was performed at 0, 1, 3, 6, and 24 h post-CCI to compare the NPC3-Gd accumulation in the brain lesion using our previous methods.^[8b,8d,9] Briefly here, mice were anesthetized with isoflurane and breathing was maintained between 50–80 breaths per minute. 10° and 30° variable flip angles were utilized to assess pre- and post-contrast R1 mapping. A bolus administration of 100 μL of NPC3-Gd with 0.1 mM Gd concentration was injected via tail vein catheter, followed by 100 μL PBS to flush all remaining NP solution from the catheter. A series of T1-weighted images was acquired over 45 min following the NPC3-Gd injection using a gradient echo sequence with a flip angle of 30°, repetition time (TR) of 54 ms, echo time (TE) of 2.73 ms, matrix size of 128 \times 128, field of view (FOV) of 20 \times 20 \times 1 mm^3 , and number of excitations (NEX) of 4, across 10 slices. A custom least squares curve fitting routine in MATLAB from the Gd concentration and R1 maps were utilized to generate K^{trans} maps, a volume transfer constant based on the changes of Gd concentration in the blood and tissue. Since K^{trans} evaluates the rate of accumulation, instead of the total accumulation of NPs, the length of developing K^{trans} was not heavily affect the rate of accumulation of NPs. The arterial input function from the R1 mapping was utilized to estimate the blood elimination half-life of NPC3 in vivo (Figure S1, Supporting Information). Arterial input function was measured from the changes in the concentration of NPC3-Gd in the blood vessel over time.

The size of each treatment group for in vivo DCE-MRI was 3 mice, except for 0- and 1-h female mice which were 6 mice each because of potential outliers at these two time points requiring new data to be generated with 3 new mice at these two time points to determine outlier status. One data point was excluded from both groups since they were counted as outliers according to Grubbs' test (Figure S2, Supporting Information). The outliers may come from estrus stage at the time of the injury, when progesterone and estrogen were at their lowest, which may lead to a higher increase in BBB leakiness compared to the female mice at other phases of estrous cycle.

Dihydroethidium Histological Analysis: The NPC3 group was intravenously administered with a bolus injection of NPC3 in Dulbecco's phosphate buffered saline (DPBS; Thermo Fisher Scientific, Waltham, MA) immediately following CCI at the concentration of 0, 0.42, 2.08, 4.17, 20.83, and 41.67 mg kg^{-1} for male mice with the average weight of 24 g and 0, 0.55, 2.76, 5.52, 27.62, and 55.25 mg kg^{-1} for female mice with the average weight of 18.1 g. The MnTMPyP group treated with an intraperitoneal bolus injection of Mn(III)tetrakis(1-methyl-4-pyridyl)porphyrin (MnTMPyP; 475 872, Sigma-Aldrich, St. Louis, MO) in DPBS (500 μL of 1 mg mL^{-1}) immediately after the CCI. The size of each treatment group was three for female mice and five for male mice. A dihydroethidium (DHE; Thermo Fisher Scientific) assay was performed as previously described with modifications.^[2b,9,10,34] Briefly, a bolus IP administration of DHE (500 μL of 1.25 mg mL^{-1}) was injected into each mouse at 3 h post-CCI. Mice were transcardially perfused at 1 h after DHE injection with ice-cold 4% paraformaldehyde (PFA) in phosphate buffer. Brain tissue was collected, fixed in 4% PFA for 24 h at 4 °C, and cryoprotected in 30% sucrose at 4 °C. The brains were then embedded in 2.6% carboxymethylcellulose, frozen, sliced coronally at a 15 μm thickness using a cryotome (Leica Biosystems CM1950, Wetzlar, Germany), placed on poly-L-lysine coated microscope slides (6 776 215, Eprexia, Kalamazoo, MI), dried overnight at RT, and stored at -80 °C until use. Sections were washed with DPBS 3 times for 5 min each, followed by water, before mounting with ProLong™ Gold Antifade Mountant (P4981001, Thermo Fisher Scientific). Images were acquired with a confocal microscope (Zeiss LSM800, Oberkochen, Germany) at an excitation wavelength of 488 nm, emission wavelength of 560–635 nm, and 5x objective lens magnification. ImageJ software was utilized to quantify the fluorescence intensity on the perilesional and the contralateral hemisphere. The perilesional region of interest (ROI) was drawn along the higher than baseline DHE intensity, while the contralateral ROI was drawn as the reflection of perilesional ROI along the midline. Since the semi-quantification of DHE was based on the mean intensity than the integral intensity, it was not expected the lesion area to impact the semi-quantification of the DHE. The representative figures of DHE, but not data quantification, were thresholded between 5 to 80 using ZEN (Zeiss). The size of each treatment group for the DHE assay was 5 mice for males and 3 mice for females. Since $n = 3$ gave enough statistical power for males and females, and 8.3 mg kg^{-1} NPC3 was administered for males and 11 mg kg^{-1} for females for Western blot and Barnes maze study, which was in the middle of the 4–20 mg kg^{-1} range for males and 5.5–27.6 mg kg^{-1} for females, the n -value of females to 5 was not increased.

Barnes Maze: As above, bolus administration of NPC3 was injected through the tail vein immediately after the CCI for the NPC3 treated group at 8.3 mg kg^{-1} for male mice and 11 mg kg^{-1} for female mice, while the CCI group did not receive any treatment after the CCI and the control group was healthy uninjured mice without treatment. The size of the treatment group was 10 control male mice, 12 untreated male CCI mice, 14 NPC3 treated male CCI mice, 9 control female mice, 10 untreated female CCI mice, and 10 NPC3 treated female CCI mice. For day 1 through 6, since there were 3 trials per day for each mouse, there were 3 times n of mice data points compared to 1 times n of mice data points for probe trial day. The maze is a 93 cm diameter platform (Noldus Information Technology, Leesburg, VA) with 20 evenly-spaced holes. At 3-weeks post-injury, the Barnes Maze was begun using the following shortened protocol. Briefly, day 0 was an acclimation day where each mouse was given 1 min to explore the maze with two 50 W lightbulbs focused on the maze and the spatial cues visible. Then, the mouse was led to the escape box using a clear, 2 L beaker and allowed to stay in the escape box for 2 min. Day 1 through 6 were comprised of 3 trials per day lasting for 3 min each trial with both lights on and spatial cues visible. At the end of each trial, the mice stayed in the escape box for 30 s. If the mice did not escape, they were led to the escape box and stayed for 30 s. On day 7, the mice were subject to a short-term trial lasting for 90 seconds with the escape box removed. Recorded videos were processed using EthoVision XT (Noldus Information Technology, Leesburg, VA).

Western Blot: The NPC3 group was treated with a bolus administration of NPC3 in DPBS (IV) immediately following the CCI, while the CCI group did not receive any treatment following the CCI. The

control group was healthy uninjured mice without any treatment. Mice were dosed within their therapeutic windows with NPC3 through tail vein injection at 8.3 mg kg⁻¹ for male mice and 11 mg kg⁻¹ for female mice, with n = 3 for each treatment group. Western blot assay was performed as previously described with modifications.^[35] Mice were transcardially perfused 1, 3, and 7 days post-CCI with ice-cold DPBS, brains were extracted, left and right cortex and hippocampus were separated and flash-frozen in liquid nitrogen and stored at -80 °C until use. Brain tissues were lysed in radioimmunoprecipitation assay (RIPA) lysis buffer containing 1 mM phenylmethylsulfonyl fluoride. Protein concentration was measured with bicinchoninic acid assay. For spectrin breakdown products (SBDPs), 5 µg of extract protein was resolved by 5–12% sodium dodecyl sulfate-polyacrylamide gel electrophoresis (SDS-PAGE) and transferred onto poly(vinylidene fluoride) (PVDF) membranes (Bio-Rad). Membranes were blocked with 3% BLOT-QuickBlocker™ (G-Biosciences, St. Louis, MO) in tris-buffered saline (TBS) for 1 h at RT and incubated overnight at 4 °C with a 1:1000 dilution of mouse anti-spectrin alpha chain (MAB1622, Sigma) and 1:1000 dilution of mouse anti-β-actin (A5441, Sigma) antibody in TBS containing 3% BLOT-QuickBlocker™ and 0.1% tween 20 (TTBS). Membranes were washed and incubated for 1 h at room temperature with 1:5000 dilution of HRP-conjugated goat anti-mouse secondary antibody (Bio-Rad) in TTBS containing 3% BLOT-QuickBlocker™. Membranes were then washed, visualized with chemiluminescence (Clarity Western ECL Substrate, Bio-Rad), and quantified with Image Lab (Bio-Rad). For lipid peroxidation products (LPOx), 30 µg of extract protein was resolved with 10% SDS-PAGE, and incubated with 1:1000 dilution of rabbit anti-4-HNE (ab46545, Abcam, Cambridge, UK), 1:1000 dilution of mouse anti-acrolein (ab240918, Abcam), 1:5000 dilution of mouse anti-β-actin, and 1:3000 dilution of goat anti-rabbit or anti-mouse secondary antibody in TTBS containing 3% BSA. 1% sodium azide was added into the blocking buffer in between different markers to deactivate the HRP, and the membrane was incubated in 1:500 dilution of goat anti-mouse IgG (ab6708, Abcam) to block the innate mouse IgG before acrolein staining. ROI was drawn on the whole lane for 4-HNE, and around 25 and 50 kDa for acrolein. The representative figures of Western blot, but not data quantification, were thresholded with Image Lab to increase contrast.

Statistical Analysis: All the data were displayed as mean ± standard deviation. A p < 0.05 was considered statistically significant. The K^{trans} and DHE quantifications were analyzed with one-way ANOVA and Dunnett's post hoc test against 0 h ipsilateral for K^{trans}, and untreated CCI mice for DHE. One-way ANOVA and Tukey's post hoc test was utilized for Western blot protein quantification because each data point was taken from different mice and the standard deviation between each time point was different depending on the fold change to the control group. The latencies in the Barnes maze were analyzed with Kaplan-Meier survival analysis and Mantel-Cox log-rank test. One-way ANOVA was utilized for intraday analysis of the Barnes maze. The similarity in slope and trend of changes in oxidative stress was analyzed using simple linear regression analysis. All statistical analysis was performed with GraphPad Prism 9 software (Graph-Pad Software, CA).

Supporting Information

Supporting Information is available from the Wiley Online Library or from the author.

Acknowledgements

The authors acknowledge grant funding from the National Institute of Neurological Disorders and Stroke of the National Institutes of Health (R01NS109488) to FK and AC. This investigation was solely the responsibility of the authors and does not necessarily represent the official views of NINDS, NIH, and NSF. This material was based upon work supported by the National Science Foundation Graduate Research Fellowship under the grant no. DGE-1610400 to HM. The authors acknowledge the Nano-Engineering Research Core facility supported by Nebraska Research Initiative fund for use of the confocal microscope.

Conflict of Interest

The authors declare no conflict of interest.

Data Availability Statement

The data that support the findings of this study are available from the corresponding author upon reasonable request.

Keywords

barnes maze, lipid peroxidation products, reactive oxygen species, spatial learning and memory, thiol functionalized nanoparticles

Received: May 23, 2023

Revised: August 4, 2023

Published online:

- [1] a) V. E. Johnson, J. E. Stewart, F. D. Begbie, J. Q. Trojanowski, D. H. Smith, W. Stewart, *Brain* **2013**, *136*, 28; b) C. Leconte, C. Benedetto, F. Lentini, K. Simon, C. Ouazizi, T. Taib, A. H. Cho, M. Plotkine, R. Mongeau, C. Marchand-Leroux, V. C. Besson, *J. Neurotrauma* **2020**, *37*, 1342; c) X. Mao, N. A. Terpolilli, A. Wehn, S. Chen, F. Hellal, B. Liu, B. Seker, N. Plesnila, *J. Neurotrauma* **2020**, *37*, 1331.
- [2] a) Z. C. Janatpour, A. Korotcov, A. Bosomtvi, B. J. Dardzinski, A. J. Symes, *J. Neurotrauma* **2019**, *36*, 3115; b) A. W. Tarudji, C. C. Gee, S. M. Romereim, A. J. Convertine, F. M. Kievit, *Biomaterials* **2021**, *272*, 120766.
- [3] a) B. Chance, H. Sies, A. Boveris, *Physiol. Rev.* **1979**, *59*, 527; b) J. St-Pierre, J. A. Buckingham, S. J. Roebuck, M. D. Brand, *J. Biol. Chem.* **2002**, *277*, 44784.
- [4] a) R. M. Adibhatla, J. F. Hatcher, *Antioxid. Redox Signaling* **2010**, *12*, 125; b) E. D. Hall, J. A. Wang, D. M. Miller, J. E. Cebak, R. L. Hill, *Neuropharmacology* **2019**, *145*, 247.
- [5] a) T. H. Liu, J. S. Beckman, B. A. Freeman, E. L. Hogan, C. Y. Hsu, *Am. J. Physiol.: Heart Circ. Physiol.* **1989**, *256*, H589; b) L. F. Marshall, A. I. Maas, S. B. Marshall, A. Bricolo, M. Fearnside, F. Iannotti, M. R. Klauber, J. Lagarrigue, R. Lobato, L. Persson, J. D. Pickard, J. Piek, F. Servadei, G. N. Wellis, G. F. Morris, E. D. Means, B. Musch, *J. Neurosurg.* **1998**, *89*, 519; c) J. P. Muizelaar, *Adv. Exp. Med. Biol.* **1994**, *366*, 389; d) J. P. Muizelaar, J. W. Kupiec, L. A. Rapp, *J. Neurosurg.* **1995**, *83*, 942; e) J. P. Muizelaar, A. Marmarou, H. F. Young, S. C. Choi, A. Wolf, R. L. Schneider, H. A. Kontos, *J. Neurosurg.* **1993**, *78*, 375.
- [6] a) V. Di Pietro, K. M. Yakoub, G. Caruso, G. Lazzarino, S. Signoretto, A. K. Barbey, B. Tavazzi, G. Lazzarino, A. Belli, A. M. Amorini, *Antioxidants* **2020**, *9*, 260; b) S. E. Gruenbaum, A. Zlotnik, B. F. Gruenbaum, D. Hersey, F. Bilotta, *CNS Drugs* **2016**, *30*, 791; c) D. S. Hersh, B. M. Ansel, H. M. Eisenberg, in *Controversies in Severe Traumatic Brain Injury Management*, **2018**, Chapter 19.
- [7] a) V. N. Bharadwaj, R. K. Rowe, J. Harrison, C. Wu, T. R. Anderson, J. Lifshitz, P. D. Adelson, V. D. Kodibagkar, S. E. Stabenfeldt, *Nanomedicine* **2018**, *14*, 2155; b) T. Higashida, C. W. Kreipke, J. A. Rafols, C. Peng, S. Schafer, P. Schafer, J. Y. Ding, D. Dornbos, X. Li, M. Guthikonda, N. F. Rossi, Y. Ding, *J. Neurosurg. Case Lessons* **2011**, *114*, 92; c) M. Grossetete, J. Phelps, L. Arko, H. Yonas, G. A. Rosenberg, *Neurosurgery* **2009**, *65*, 702.
- [8] a) J. L. Xu, M. Ypma, P. A. Chiarelli, J. Park, R. G. Ellenbogen, P. S. Stayton, P. D. Mourad, D. Lee, A. J. Convertine, F. M. Kievit, *Adv. Funct. Mater.* **2016**, *26*, 4124; b) H. A. Miller, A. W. Magsam, A. W. Tarudji, S. Romanova, L. Weber, C. C. Gee, G. L. Madsen, T. K. Bronich, F. M. Kievit, *Sci. Rep.* **2019**, *9*, 16099; c) V. N. Bharadwaj, J. Lifshitz, P. D.

- Adelson, V. D. Kodibagkar, S. E. Stabenfeldt, *Sci. Rep.* **2016**, *6*, 29988; d) B. A. Bony, H. A. Miller, A. W. Tarudji, C. C. Gee, A. Sarella, M. G. Nichols, F. M. Kievit, *ACS Omega* **2020**, *5*, 16220; e) L. J. Cruz, M. A. Stammes, I. Que, E. R. van Beek, V. T. Knol-Blankevoort, T. J. A. Snoeks, A. Chan, E. L. Kaijzel, C. W. G. M. Löwik, *J. Controlled Release* **2016**, *223*, 31; f) Z. S. Bailey, E. Nilson, J. A. Bates, A. Oyalowo, K. S. Hockey, V. S. S. Sajja, C. Thorpe, H. Rogers, B. Dunn, A. S. Frey, M. J. Billings, C. A. Sholar, A. Hermundstad, C. Kumar, P. J. VandeVord, B. A. Rzigalinski, *J. Neurotrauma* **2020**, *37*, 1452; g) H. Alluri, C. A. Shaji, M. L. Davis, B. Tharakan, in *Traumatic and Ischemic Injury*, **2018**; h) M. K. Başkaya, A. Muralikrishna Rao, A. Doğan, D. Donaldson, R. J. Dempsey, *Neurosci. Lett.* **1997**, *226*, 33; i) W. Li, L. Watts, J. Long, W. Zhou, Q. Shen, Z. Jiang, Y. Li, T. Q. Duong, *Brain Res.* **2016**, *1646*, 53; j) Y.-L. Liu, Z.-M. Xu, G.-Y. Yang, D.-X. Yang, J. Ding, H. Chen, F. Yuan, H.-L. Tian, *Acta Pharmacol. Sin.* **2017**, *38*, 1445; k) V. N. Bharadwaj, C. Copeland, E. Mathew, J. Newbern, T. R. Anderson, J. Lifshitz, V. D. Kodibagkar, S. E. Stabenfeldt, *Tissue Eng. Part A* **2020**, *26*, 688.
- [9] A. Priestler, R. Waters, A. Abbott, K. Hilmas, K. Woelk, H. A. Miller, A. W. Tarudji, C. C. Gee, B. McDonald, F. M. Kievit, A. J. Convertine, *Biomacromolecules* **2022**, *23*, 1703.
- [10] A. W. Tarudji, H. A. Miller, E. T. Curtis, C. L. Porter, G. L. Madsen, F. M. Kievit, *J. Controlled Release* **2023**, *355*, 149.
- [11] a) O. Mair, F. Greve, R. Lefering, P. Biberthaler, M. Hanschen, D. G. U. TraumaRegister, *Front. Neurosci.* **2022**, *16*, 974519; b) R. P. Gupta, W. M. Brooks, R. R. Vukas, J. D. Pierce, J. L. Harris, *J. Neurotrauma* **2019**, *36*, 3063.
- [12] F. C. Goldstein, A. F. Caveney, V. S. Hertzberg, R. Silbergleit, S. D. Yeatts, Y. Y. Palesch, H. S. Levin, D. W. Wright, *J. Neurotrauma* **2017**, *34*, 115.
- [13] D. Yoo, A. W. Magsam, A. M. Kelly, P. S. Stayton, F. M. Kievit, A. J. Convertine, *ACS Nano* **2017**, *11*, 8600.
- [14] a) Z. S. Bailey, E. Nilson, J. A. Bates, A. Oyalowo, K. S. Hockey, V. Sajja, C. Thorpe, H. Rogers, B. Dunn, A. S. Frey, M. J. Billings, C. A. Sholar, A. Hermundstad, C. Kumar, P. J. VandeVord, B. A. Rzigalinski, *J. Neurotrauma* **2020**, *37*, 1452; b) M. Rashno, A. Sarkaki, Y. Farbood, M. Rashno, L. Khorsandi, M. K. G. Naseri, M. Dianat, *Life Sci.* **2019**, *228*, 285; c) J. Fang, H. Wang, J. Zhou, W. Dai, Y. Zhu, Y. Zhou, X. Wang, M. Zhou, *Drug Des. Devel. Ther.* **2018**, *12*, 2497; d) T. Cheng, W. Wang, Q. Li, X. Han, J. Xing, C. Qi, X. Lan, J. Wan, A. Potts, F. Guan, J. Wang, *Free Radic. Biol. Med.* **2016**, *92*, 15; e) C. Cui, C. Wang, F. Jin, M. Yang, L. Kong, W. Han, P. Jiang, *Mol. Med.* **2021**, *27*, 118; f) J. M. McCord, *Dose Response* **2008**, *6*, dose.
- [15] H. Esterbauer, R. J. Schaur, H. Zollner, *Free Radic. Biol. Med.* **1991**, *11*, 81.
- [16] R. L. Hill, I. N. Singh, J. A. Wang, E. D. Hall, *Neurochem. Int.* **2017**, *111*, 45.
- [17] K. K. W. Wang, R. Posmantur, R. Nath, K. McGinnis, M. Whitton, R. V. Talanian, S. B. Glantz, J. S. Morrow, *J. Biol. Chem.* **1998**, *273*, 22490.
- [18] R. T. Gerlai, A. McNamara, S. Williams, H. S. Phillips, *Brain Res. Bull.* **2002**, *57*, 3.
- [19] a) M. Lamtai, J. Chaibat, S. Ouakki, O. Zghari, A. Mesfioui, A. El Hessni, E. H. Rifi, I. Marmouzi, A. Essamri, A. Ouichou, *Brain Sci.* **2018**, *8*, 141; b) P. Gaignard, S. Savouroux, P. Liere, A. Pianos, P. Thérond, M. Schumacher, A. Slama, R. Guennoun, *Endocrinology* **2015**, *156*, 2893; c) M. Das, R. Dixit, P. K. Seth, H. Mukhtar, *J. Neurochem.* **1981**, *36*, 1439; d) M. Y. Chou, Y. J. Chen, L. H. Lin, Y. Nakao, A. L. Lim, M. F. Wang, S. M. Yong, *Nutrients* **2019**, *11*, 1870.
- [20] a) M. Benhar, *Antioxidants* **2020**, *9*, 309; b) A. Sharma, K. Liaw, R. Sharma, Z. Zhang, S. Kannan, R. M. Kannan, *Theranostics* **2018**, *8*, 5529; c) K. Ulrich, U. Jakob, *Free Radic. Biol. Med.* **2019**, *140*, 14.
- [21] M. Mohamadpour, K. Whitney, P. J. Bergold, *Front Neurosci.* **2019**, *13*, 07.
- [22] R. Duvdevani, R. L. Roof, Z. Fülöp, S. W. Hoffman, D. G. Stein, *J. Neurotrauma* **1995**, *12*, 65.
- [23] A. P. Mann, P. Scodeller, S. Hussain, J. Joo, E. Kwon, G. B. Braun, T. Mölder, Z.-G. She, V. R. Kotamraju, B. Ranscht, S. Krajewski, T. Teesalu, S. Bhatia, M. J. Sailor, E. Ruoslahti, *Nat. Commun.* **2016**, *7*, 11980.
- [24] H.-P. Simmen, A. Zimmerman, S. Fox, R. Griffin, T. Nelp, E. B. A. F. Thomaz, M. Mvungi, B. T. Mmbaga, F. Sakita, C. J. Gerardo, J. R. N. Vissoci, C. A. Staton, *PLoS One* **2020**, *15*, 0240528.
- [25] M. A. Ansari, K. N. Roberts, S. W. Scheff, *Free Radic. Biol. Med.* **2008**, *45*, 443.
- [26] D. L. Brody, D. M. Holtzman, *Exp. Neurol.* **2006**, *197*, 330.
- [27] K. Gawel, E. Gibula, M. Marszalek-Grabska, J. Filarowska, J. H. Kotlinska, *Naunyn-Schmiedeberg Arch. Pharmacol.* **2019**, *392*, 1.
- [28] L. F. Marshall, A. I. R. Maas, S. B. Marshall, A. Bricolo, M. Fearnside, F. Iannotti, M. R. Klauber, J. Lagarrigue, R. Lobato, L. Persson, J. D. Pickard, J. Piek, F. Servadei, G. N. Wellis, G. F. Morris, E. D. Means, B. Musch, *J. Neurosurg. Case Lessons* **1998**, *89*, 519.
- [29] a) X. Niu, S. Zheng, H. Liu, S. Li, *Mol. Med. Rep.* **2018**, *18*, 4516; b) J. Xu, H. Wang, K. Ding, L. Zhang, C. Wang, T. Li, W. Wei, X. Lu, *Free Radic. Biol. Med.* **2014**, *71*, 186.
- [30] M. E. Schober, D. F. Requena, L. J. Davis, R. R. Metzger, K. S. Bennett, D. Morita, C. Niedzwecki, Z. Yang, K. K. Wang, *Brain Res.* **2014**, *1574*, 105.
- [31] a) H. M. Bramlett, W. D. Dietrich, *J. Neurotrauma* **2001**, *18*, 891; b) C. M. Monaco, V. V. Mattioli, K. A. Folweiler, J. K. Tay, N. K. Yelleswarapu, L. M. Curatolo, A. M. Matter, J. P. Cheng, A. E. Kline, *Exp. Neurol.* **2013**, *247*, 410; c) L. B. Tucker, A. H. Fu, J. T. McCabe, *J. Neurotrauma* **2016**, *33*, 880; d) L. B. Tucker, J. F. Burke, A. H. Fu, J. T. McCabe, *J. Neurotrauma* **2017**, *34*, 890; e) S. J. Doran, R. M. Ritzel, E. P. Glaser, R. J. Henry, A. I. Faden, D. J. Loane, *J. Neurotrauma* **2019**, *36*, 1040.
- [32] a) R. L. Roof, R. Duvdevani, D. G. Stein, *Brain Res.* **1993**, *607*, 333; b) C. A. O'Connor, I. Cernak, R. Vink, *Brain Res.* **2005**, *1062*, 171; c) R. L. Roof, E. D. Hall, *J. Neurotrauma* **2000**, *17*, 1155; d) A. Razmara, S. P. Duckles, D. N. Krause, V. Procaccio, *Brain Res.* **2007**, *1176*, 71; e) M. Torrens-Mas, D.-G. Pons, J. Sastre-Serra, J. Oliver, P. Roca, *Redox Biol.* **2020**, *31*, 101505.
- [33] W. Zhao, Q. Li, Y. Ma, Z. Wang, B. Fan, X. Zhai, M. Hu, Q. Wang, M. Zhang, C. Zhang, Y. Qin, S. Sha, Z. Gan, F. Ye, Y. Xia, G. Zhang, L. Yang, S. Zou, Z. Xu, S. Xia, Y. Yu, M. Abdul, J.-X. Yang, J.-L. Cao, F. Zhou, H. Zhang, *Front Neurosci.* **2021**, *15*, 650793.
- [34] E. M. Lutton, R. Razmpour, A. M. Andrews, L. A. Cannella, Y.-J. Son, V. V. Shuvaev, V. R. Muzykantov, S. H. Ramirez, *Sci. Rep.* **2017**, *7*, 3846.
- [35] B. A. Bony, A. W. Tarudji, H. A. Miller, S. Gowrikumar, S. Roy, E. T. Curtis, C. C. Gee, A. Vecchio, P. Dhawan, F. M. Kievit, *ACS Nano* **2021**, *15*, 18520.